High positronium yield and emission into the vacuum from oxidized tunable nanochannels in silicon

S. Mariazzi,[1,*] P. Bettotti,[2] S. Larcheri,[2] L. Toniutti,[1] and R. S. Brusa[1]
[1]*Dipartimento di Fisica, Università di Trento and INFN, Gruppo Collegato di Trento, Via Sommarive 14, Povo, I-38050 Trento, Italy*
[2]*Laboratorio di Nanoscienze, Dipartimento di Fisica, Università di Trento, Via Sommarive 14, Povo, I-38050 Trento, Italy*
(Received 18 February 2010; published 10 June 2010)

A positron-positronium converter composed of regular nanochannels with size in the 5–100 nm range and length about 2 μm has been produced in silicon by electrochemical etching. After controlled oxidation of the inner surface of the channels, a positronium yield up to 45% of the positrons implanted at 1 keV energy was observed. At 1 keV positron implantation energy about 42% of positronium is estimated to be emitted into the vacuum. At 10 keV positron implantation energy, corresponding to a depth of ~800 nm, the positronium fraction emitted into the vacuum is still 10% in a sample with channels of 4–7 nm and up to 23–25 % in samples with larger channels. The positronium diffusion length and the fast positronium fraction emitted into the vacuum have been investigated as a function of the channel size tuned in the 5–100 nm range. The dependence of the positronium cooling from the size of the nanochannel is discussed and an evaluation of the expected fraction of thermalized orthopositronium in vacuum is given.

DOI: 10.1103/PhysRevB.81.235418 PACS number(s): 36.10.Dr, 78.70.Bj, 61.46.−w

I. INTRODUCTION

Positronium (Ps) is a quasistable hydrogenlike bound state of an electron and its antiparticle, the positron (e^+).[1] Ps can exist in two different states: the singlet state, parapositronium (*p*-Ps) (total spin 0, formation probability $\frac{1}{4}$) and the triplet state, orthopositronium (*o*-Ps) (total spin 1, formation probability $\frac{3}{4}$). In vacuum *p*-Ps decays into 2γ rays with a mean lifetime of 125 ps while *o*-Ps decays into 3γ rays with a mean lifetime of 142 ns.

Ps can be obtained by implanting in solids positrons with energy of few kiloelectron volts.[2] In metals and semiconductors, the high electron density prevents the formation of Ps in the bulk. In these materials, Ps yield can occur only at the surface where a thermalized positron diffusing back to the surface can capture an electron and be emitted as Ps.[3] Conversely in insulators, Ps formation at the surface is usually hindered but Ps can be formed in the bulk. After formation Ps can diffuse toward the surface and be released into the vacuum if its work function is negative.[3] In porous insulator materials Ps is also emitted into internal porosities of nanometric or subnanometric size. In these nanovoids the *o*-Ps lifetime is reduced by the pickoff annihilation: in the pickoff process, the positron of the *o*-Ps annihilates via 2γ with an electron of the walls of the pores. Nevertheless, if pores are connected to the surface, a fraction of *o*-Ps can escape into the vacuum after diffusion through the porosities.

The study of the *o*-Ps lifetime, *o*-Ps 3γ annihilation, and *o*-Ps velocity when it is emitted into vacuum is becoming an important tool for characterizing dimension, distribution, shape, and connectivity of pores in insulator materials.[4,5] On the other hand, Ps formation and emission into pores is also of great interest in fundamental physics. The formation of Ps_2 has been observed in porous silica after implantation of burst of many positrons.[6,7] Confinement of 10^{17}–10^{18} *o*-Ps/cm^3 in nanometric cavities at temperatures below 30 K would allow to observe the *o*-Ps Bose-Einstein condensation (*o*-Ps-BEC).[8,9] *o*-Ps-BEC would open the route for other interesting linked experiments as making plane-wave monoenergetic *o*-Ps beam (*o*-Ps atom laser) and *o*-Ps annihilation gamma ray laser.[10] The realization of beams of cold *o*-Ps (*o*-Ps temperature <160 K) obtained by implanting burst of positrons in materials with porosity connected toward the surface have been proposed for high-precision spectroscopy studies and production of antihydrogen by charge-exchange process with antiprotons.[11,12]

Up to now several experiments carried out on different silica-based porous materials have shown that at room temperature the kinetic energy of a fraction of *o*-Ps can be reduced close to thermal energy by *o*-Ps collisions with the wall of the pores and *o*-Ps can be finally emitted into the vacuum within its lifetime of 142 ns.[13–18]

For all the mentioned applications, porous materials with very high *o*-Ps yield and abundant emission of *o*-Ps into the vacuum are required. In this context, porous-based silica materials are the most widely explored. The reason is that in silica a high percentage of implanted positrons forms Ps (Ref. 19) and in presence of porosity connected to the surface *o*-Ps can be emitted into the vacuum.[20,21] Moreover, in the last decade the ability to realize mesopores with different dimension and shape in silica-based films is remarkably improved (see for instance Ref. 22).

In the present work we study the *o*-Ps emission characteristics (Ps yield, fast fraction of Ps emission, and Ps diffusion length) into the vacuum from an innovative target composed of a nanochannel array etched into a silicon substrate. This material offers many advantages compared with disordered porous silica sol-gel-based materials. The most important are the possibility of a nanometer tuning of the pores size, the ordered structure (roughly composed of parallel pores extending perpendicular to the surface plane), the greater mechanical stability, and the easier fabrication process. The study was carried out with two positron annihilation spectroscopy (PAS) techniques: 2γ-3γ annihilation ratio of positronium (3γ-PAS) performed with a continuous positron beam and positron annihilation lifetime spectroscopy (PALS)

executed with a pulsed positron beam.[3,23,24] Samples were depth profiled by implanting positrons with a variable energy. With 3γ-PAS the fraction of *o*-Ps annihilating into three gamma rays can be measured. PALS allows the measurement of the fraction of *o*-Ps annihilating by pickoff and its reduced lifetime.

A high yield and emission into the vacuum of *o*-Ps was obtained after an appropriate thermal oxidation of the inner surface of the channels. This nanostructured material allows a higher *o*-Ps emission[25] than in the disordered silica based materials for positron implantation energy above 3 keV.[21] The effects of the nanochannel dimensions on *o*-Ps out-diffusion toward the vacuum are studied and a strong correlation between the nanochannel size, the velocity of emitted *o*-Ps, and the *o*-Ps diffusion length is evidenced. The importance of tuning the dimension of nanochannels for cooling *o*-Ps below room temperature will be discussed.[26]

II. EXPERIMENTAL

Nanochannels perpendicular to the Si surface can be obtained by electrochemical etching of Si in hydrofluoric acid (HF) solution.[27] The properties of pores as density, diameter, and length depend on anodization conditions as HF concentration, etching current, silicon type and resistivity, and anodization duration. In the last two decades these kind of samples has been investigated for their morphology and striking photoluminescence properties that make them attractive for the realization of sensors and light-emitting devices.[27] In the former case the key parameter to be optimized is the surface area while in the latter case the interest is in the optimum control over the silicon nanopillars, responsible of the photoluminescent behavior. In both cases the resulting materials are composed of nanochannels with diameter from tens to hundreds of nanometer. In this work we are interested in maximizing the yield of *o*-Ps, which is expected to depend on the ratio between the volume of the inner silicon pillar and the surface silica layer, and on the pore size. Thus, we have explored a completely different porosity regime, obtaining nanochannels with smaller diameters in the 5–20 nm range and extending for few micrometer in depth by optimizing all the above production parameters. Si *p*-type (100) wafers with resistivity between 0.15 and 0.21 Ω cm, etching current in the 10–30 $\mathrm{mA/cm^2}$ range and anodization duration in the 10–20 min range were used. The etching solution was realized by adding absolute ethanol to a commercial aqueous solution at 48% of HF with volume ratio of 1:3=HF:ethanol.

After the electrochemical etching, the samples were cleaned in absolute ethanol $\geq$99.8%. A first sample was transferred in a vacuum chamber and the pressure was reduced to 10^{-9} torr to prevent the oxidation of the nanochannel walls of immediately after their synthesis. In the following we will indicate this sample as not oxidized. The inner surfaces of nanochannels in a freshly etched sample are almost totally covered by SiH_x groups but hydrogen is progressively released and more stable SiO_x complexes begins to be formed after short exposition to ambient air.[27] The other samples were oxidized in air at temperature ranging from 100 to 400 °C for different times. Since the highest *o*-Ps yield has been observed after thermal treatment at 100 °C for 2 h, a series of six samples was realized using these parameters. The samples of this series were subjected to a different number of etchings in HF etching solution for 1 min and a reoxidation in air at 100 °C for 2 h. The samples prepared using this technique will be labeled #0, #1, #2, #3, #4, and #5 where the progressive number indicates the number of cycles of etching and subsequently reoxidation, the sample was subjected to. The aim of this procedure of etching and reoxidation was the individuation of a technique that enables us to enlarge the diameter of the pores without changing their density and the regularity of the nanochannels.

It must be noticed that the surface of the samples of the nanochannels produced by electrochemical etching is highly chemically reactive immediately after the production.[27] The passivation of the surface realized with the oxidation in air makes the sample and the *o*-Ps formation and emission stable for many weeks if the samples are maintained in vacuum. Conversely, if the samples are stored in air the contamination of the inner channel surface reduces the *o*-Ps yield in a few days.

The formation of *o*-Ps and its out-diffusion through nanochannels was analyzed in a sample layer of ~ 3 μm from the surface, by 2γ-3γ annihilation ratio of positronium (3γ-PAS) measurements. The depth profiling was carried out using a slow positron beam[28] changing the positron implantation energy E from 0.06 to 25 keV. At positron implantation energies higher than 0.5 keV the beam spot on the sample was about 1 mm in diameter, 2–3 mm at the lowest energies. Particles backscattered or emitted from the surface of the target can fly for more than 10 cm before hitting the walls of the chamber. Channeling effects through the nanochannels are minimized because positrons are focused at the target. Nevertheless the regularity of open and solid space in this sample is expected to have influence on the slowing down of injected positrons. As a first approximation we assumed the Makovian profile for implanted positrons.[3] It relates the mean positron implantation depth z to the positron implantation energy E through the equation $z=\frac{40}{\rho}E^{1.6}$ with z in nanometers when the material density ρ (1.9 $\mathrm{g/cm^3}$ as estimated for the silicon layer with nanochannels) and energy E are expressed in grams per cubic centimeter and kiloelectron volt, respectively.[3] An *a posteriori* check shows that the fitting of the measured data correctly locates the boundary between the nanochannel region and the bulk silicon. A possible broadening of the positron implantation profile, simulated as a change in material density, could affect our length scale by about 5–10 %.

The annihilation gamma rays were detected by two high-purity germanium (HpGe) detectors in a 180° configuration at a distance of about 4 cm from the samples. The two HpGe detectors had 45% efficiency and 1.4 keV energy resolution at 511 keV.[29,30] The annihilation spectra were acquired with 2 μs shaping time in the amplifier and an energy resolution of 64 eV for channel. The distribution of the annihilation γ-ray energy (E_γ) was subdivided into two regions: the 511 keV peak area (P) attributable prevalently to 2γ annihilation ($|511-E_\gamma| \leq 4.25$ keV) and the valley area (V) due to *o*-Ps

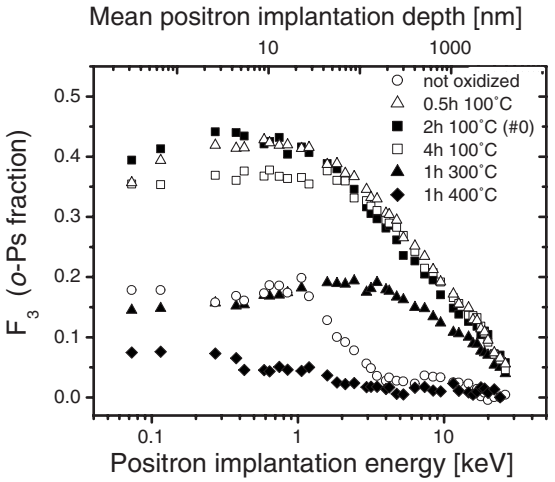

FIG. 1. Fraction $F_{3\gamma}$ of implanted positrons annihilating as o-Ps vs positron implantation energy (lower scale) and mean positron implantation depth (upper scale). Samples with nanochannels: not oxidized, oxidized at different times and different temperatures. The error on $F_{3\gamma}(E)$ points is −3.5% and +0.5%.

3γ annihilation ($410 \leq E_\gamma \leq 500$ keV). The 2–3 gamma ratio of Ps, $R(E)$ parameter, was calculated as the ratio between the valley area and the peak area at each positron implantation energy E. The $R(E)=V(E)/P(E)$ parameter was calibrated by measuring the Ps formation in a Ge crystal as a function of the temperature.[30,31] The calibrated fraction of implanted positron annihilating as o-Ps is defined as $F_{3\gamma}(E)=\frac{3}{4}\{1+\frac{P_1[R_1-R(E)]}{P_0[R(E)-R_0]}\}^{-1}$,[32] where R_1 (100% positronium formation) is the value obtained by extrapolating to zero implantation energy the $R(E)$ curve measured in Ge held at 1000 K. R_0 (0% positronium formation) was assumed as the value of $R(E)$ at the highest positron implantation energy. P_0 and P_1 are the values of the 511 keV peak area obtained at 0% and 100% o-Ps formation, respectively.[31,33]

PALS measurements were done with the pulsed low-energy positron system (PLEPS)[34] at the high intense Neutron induced POsitron source MUniCh (NEPOMUC).[35] The overall (detector plus pulsing system) time resolution was 330 ps. These measurements were done on a sample to acquire information on the positron and positronium annihilations inside the channels.

The size of nanochannels has been evaluated by scanning electron microscopy (SEM) analysis of the surface of the samples. SEM measurements have been carried out by a high-resolution JEOL JSM-7001F thermal field-emission scanning electron microscope. Accelerating voltage ranges from 0.5 to 30 kV and its resolution is 1.2 nm at 30 kV. These analyses have been carried out without the need to coat the samples with metal or carbon for conductivity.

III. RESULTS AND DISCUSSION

A. Nanochannels oxidation for optimizing o-Ps yield

The fraction $F_{3\gamma}(E)$ of implanted positrons annihilating as o-Ps vs positron implantation energy E is shown in Fig. 1 for the not oxidized sample and the samples in which oxidation in air was carried out at different temperatures and for different times. The error on $F_{3\gamma}(E)$ points due to calibration of Ps yield is estimated to be −3.5% and +0.5%. The error takes into consideration that for Ge crystal, used for calibration, the total Ps yield at the surface is expected to be near to 97%.[33] In the not oxidized sample, o-Ps was observed for positron implantation energy lower than 1 keV, energy corresponding to a depth less than ~20 nm. At higher positron implantation energy the $F_{3\gamma}(E)$ fraction decreases quickly toward zero. The not oxidized sample was exposed to air just for few minutes between the production of the nanochannels and the insertion of the sample in the vacuum chamber. Because of the oxygen is known to be progressively adsorbed in these samples after a few minutes of permanence in ambient air,[27] the observed Ps formation can be ascribed to the starting oxidation of the channels from the surface. As a matter of fact, o-Ps can be formed with high yield both in amorphous as crystalline silica[36] but no o-Ps formation was observed to occur at the clean surface of buried cavities in silicon p type[37] and very low o-Ps yield takes place at silicon surface.[31]

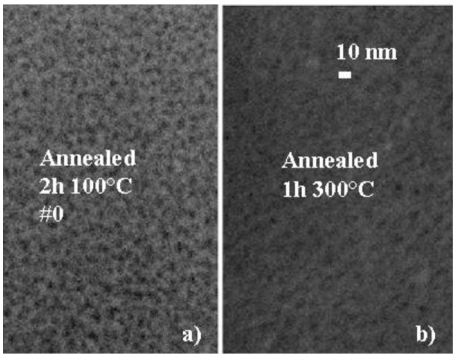

FIG. 2. SEM pictures of the surface of samples annealed in air: (a) 2 h at 100 °C (sample #0) and (b) 1 h 300 °C.

The yield of o-Ps was found to be strongly dependent on the chosen temperature for the oxidation by thermal annealing in air. High amount of o-Ps is evidenced after thermal annealing at 100 °C. Lower values of $F_{3\gamma}(E)$ were observed after annealing at 300 °C. Thermal treatment at 400 °C hindered almost completely the o-Ps annihilation via 3γ (see Fig. 1). SEM pictures show that in samples annealed 2 h at 100 °C the diameter of nanochannels ranges from 4 to 7 nm and the distance between adjacent pores is comparable to their dimension [Fig. 2(a)]. After annealing at 300 °C many channels seem to be completely filled by silica grown [Fig. 2(b)]. The reduction in pore dimensions after annealing at temperature higher than 100 °C, or their complete filling, has to be considered the cause of the reduction in o-Ps fraction out diffusing from the channels.

Among the samples annealed at 100 °C, the highest values of $F_{3\gamma}(E)$ were obtained after 2 h of thermal treatment. In this case the fraction of implanted positron annihilating as o-Ps reached a maximum of 45% around 1 keV positron implantation energy. A slightly lower value (~42%) was observed in nanochannels oxidized for 0.5 h while a longer thermal treatment of 4 h reduced the o-Ps fraction to less than 38%. The sample annealed for 0.5 h at 100 °C showed

slightly higher values of $F_{3\gamma}(E)$ at positron implantation energies higher than 2 keV (Fig. 1).

The mechanism which gives the high yield of observed positronium in these samples requires a discussion. The volume occupied by the channels can be estimated less than about half of the total volume in the ~2 μm etched silicon layer. The silicon oxide layer on the inner walls of the channels is expected to have a thickness of few nanometers. A simple geometrical evaluation, assuming the sample composed of regular cylindrical channels, shows that the total bulk silica in the sample does not exceed 10% of the total volume. Therefore, the observed Ps cannot be only formed by positrons stopped in the silica layers during their slowing down. The high amount of *o*-Ps must be correlated with positrons that diffuse in silicon, reach the silicon/silica interface, and pass in the silicon oxide layer because energetically favored.[38] Since the e^+ diffusion length in silicon *p* type is around 200–250 nm (Ref. 3) while the distance among the pores is extremely shorter (few nanometers), a large fraction of implanted positrons is expected to reach the silicon/silica interface. Here Ps can be formed and, after a short diffusion path, be emitted into the nanochannels. Ps formed in silica was found to be emitted in vacuum with two-energy distribution centered at 1 and 3 eV.[36] Hereafter the sample with the highest *o*-Ps yield, i.e., the sample thermal treated at 100 °C, will be analyzed in details.

B. *o*-Ps yield vs nanochannel dimensions

As mentioned, a procedure of etching and reoxidation was applied to the sample treated at 100 °C for increasing the channel dimensions without losing in the density of channels for unit area. In Fig. 3 the $F_{3\gamma}(E)$ curves obtained measuring samples labeled #0, #1, #2, #3, #4, and #5 are shown. The progressive number indicates the number of etching and oxidation cycles.

The thickness of the silicon region with nanochannels is around 2 μm (vertical line in Fig. 3). If the samples are subjected to etching and reoxidation cycles, the region of the silicon with nanochannels does not change but their diameter tends to increase cycle after cycle as pointed out by the SEM images reported in Fig. 4. The size of nanochannels can be estimated to be around 4–7 nm in sample #0 and 8–12 nm, 8–14 nm, 10–16 nm, 14–20 nm, and 80–120 nm in samples #1, #2, #3, #4 and #5, respectively.

At each positron implantation energy the *o*-Ps fraction, $F_{3\gamma}(E)$, is composed of two contributions: the first one given by the *o*-Ps that annihilates into three gammas inside the channels and the second one given by *o*-Ps that escapes into the vacuum. Large amount of *o*-Ps emission into the vacuum from a sample of this type (nanochannels dimensions in the 5–8 nm range) was recently directly observed by time of flight (TOF) measurements (Ref. 25). A fraction of *o*-Ps was found to escape with thermal energy from a mean positron implantation depth of ~470 nm (7 keV implantation energy) at RT and at cryogenic temperature of 200 and 150 K. The escaping from such a large depth was allowed because of the high *o*-Ps diffusion length. The TOF results on *o*-Ps outdiffusion were consistent with the 3γ-PAS finding on the same sample.

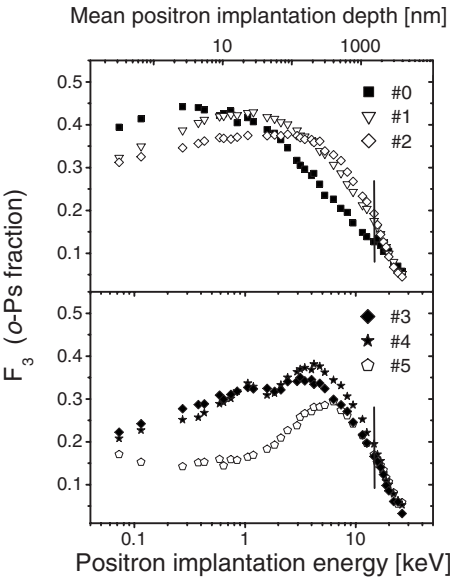

FIG. 3. Fraction $F_{3\gamma}$ of implanted positrons annihilating as *o*-Ps vs positron implantation energy (lower scale) and mean positron implantation depth (upper scale). Samples realized with a different number of etching and reoxidation cycles (#0, #1, #2, #3, #4, and #5) in air at 100 °C for 2 h. The vertical lines mark the border between the silicon region with nanochannels and the bulk silicon. The error on $F_{3\gamma}(E)$ points is −3.5% and +0.5%.

The maximum yield of *o*-Ps is about 45% in samples #0, then it decreases progressively reaching about 35% in sample #4 and 30% in sample #5. This maximum is reached at increasing positron implantation energy going from sample #0 to sample #5. In spite of this progressive decrease in the maximum yield, at 10 keV positron implantation energy the *o*-Ps yield is about the same (23–25 %) in all the cycled samples.

As appreciable from Fig. 3, the $F_{3\gamma}(E)$ values below 3–5 keV positron implantation energy show a decrease. In samples #3, #4, and #5 this decrease is more marked than in samples #0, #1, and #2. In sample #5, where the size of nanochannels becomes larger than in #4 by six times, the

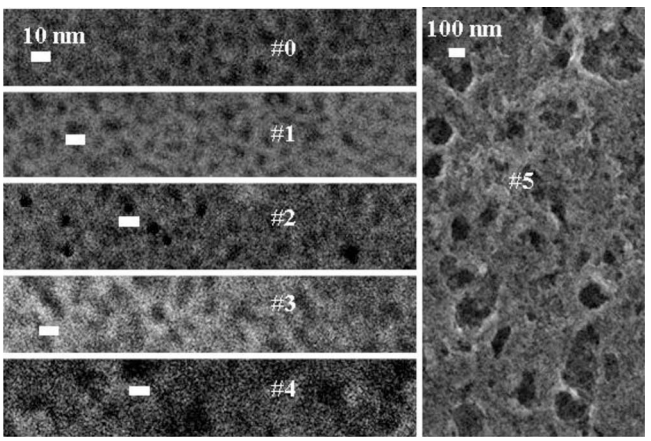

FIG. 4. SEM pictures of the surface of samples #0, #1, #2, #3, #4, and #5. The scale of sample #5 is ten times that of the other samples. Numbers refer to the etching and reoxidation cycles.

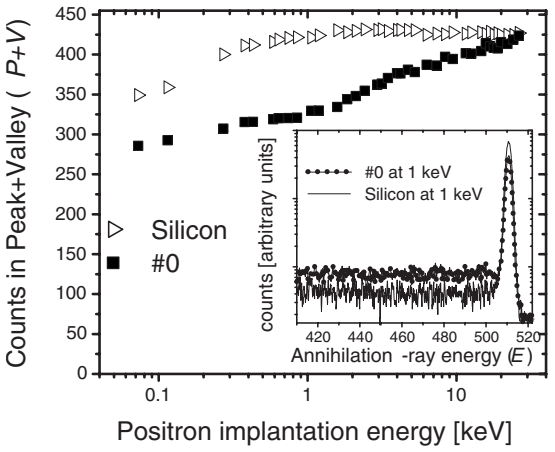

FIG. 5. Sum of the counts in the peak and in the valley area $(P+V)$ in the unit of time vs positron implantation energy as measured in a silicon sample and in sample #0. Inset: comparison between energy spectra measured in #0 and in silicon at 1 keV positron implantation energy; counts in logarithmic scale.

$F_{3\gamma}(E)$ decreasing is steeper and more noticeable. The lower $F_{3\gamma}(E)$ values observed in these samples at low positron implantation energies must be attributed to a decrease in the detection efficiency of the HpGe detectors. In fact, in larger nanochannels, a higher fraction of *o*-Ps escapes into the vacuum after only few collisions with walls and hence with a higher kinetics energy.[26,39] These *o*-Ps atoms fly and annihilate far away from the HpGe detectors. This effect can be investigated more in detail as described in the following and it gives comparative information on the escaping of fast *o*-Ps in the different samples. Moreover it will be shown that it is possible to correct the curves of Fig. 3 for the not-detected *o*-Ps, and then to fit these data to extract information on the out diffusing *o*-Ps fraction and on the *o*-Ps diffusion length L_{Ps}.

C. Escaping of fast *o*-Ps vs nanochannel dimension

In the inset of Fig. 5, energy spectra measured at 1 keV in a Si *p* type (100) and in sample #0 are shown. An increase in counts in the valley area and a decrease in counts in the 511 keV peak due to *o*-Ps 3γ annihilation can be clearly observed in sample #0 with respect to Si sample. The sum of the counts in the peak and in the valley areas $[P(E)+V(E)]$ in the unit of time, as measured in the Si sample as a function of the positron implantation energy, is reported in Fig. 5. Due to the transmission function of the present apparatus,[28,29] the counts are practically constant for positron implantation energy higher than 0.3 keV. The value of $P(E)+V(E)$ as measured in the sample #0 and reported in the same figure has a different behavior as a function of E. It starts from very low values and increases gradually with the increasing of the positron implantation energy. At 25 keV the value of $P(E)+V(E)$ in #0 approaches to the constant value measured in silicon. This loss of counts with respect to silicon can be ascribed to (a) gammas emitted by 3γ *o*-Ps annihilations with energy out both of the selected peak and valley windows, (b) the emission of *o*-Ps or positrons into the vacuum that fly away from the sample and annihilate in a region where the detection efficiency of the HpGe detectors is lower due to the solid angle. Therefore, in a sample like #0 the counts in the peak and in the valley can be written, respectively, as

$$P(E) = P_{\mathrm{Si}} - N_{escaped}(E) - N_{2\gamma 3\gamma}(E),$$

$$V(E) = V_{\mathrm{Si}} + \frac{N_{2\gamma 3\gamma}(E)}{\alpha}, \tag{1}$$

where P_{Si} and V_{Si} are the constant values of the peak and valley areas measured in silicon in the unit of time, $N_{2\gamma 3\gamma}(E)$ is the number of counts that disappear from the peak area due to the annihilations of *o*-Ps via 3γ, and α is a constant parameter which takes into account that only a fraction of $N_{2\gamma 3\gamma}(E)$ is recorded in the valley area. Finally, $N_{escaped}(E)$ is the number of counts that disappear from the peak area due to positrons or *o*-Ps atoms emitted with high velocity and are not detected because flying far from the sample region. The emission of positrons into the vacuum is due to the presence of epithermal and backscattered e^+ from the surface but both these contributions are expected to be small. The diffusion length of epithermal positrons before their thermalization at energy below the positron work function in a Si/SiO_2 system is 2.4 nm,[40] shorter than the distance between adjacent pores in our sample (4–7 nm). Thus few e^+ can be emitted in a channel with epithermal energy and a smaller fraction can out diffuse through the nanochannels keeping its energy. The fraction of implanted positrons backscattered from the surface of a sample depends on the atomic number of the material Z and on the e^+ implantation energy. In particular, in materials with Z comparable to that of silicon, the fraction of backscattered positrons has been found to be about 5% and constant up to 20–30 keV positron implantation energy.[41] Consequently, the fraction of backscattered e^+ is expected to be roughly the same in silicon and in samples that are constituted prevalently of silicon. There is also a fraction of fast Ps atoms with energy ranging from 10 to 40 eV, formed by backscattered positrons.[42] Also this component is expected to be about the same in silicon and etched silicon. In conclusion the fractions of epithermal, backscattered positrons, and fast Ps from backscattered positrons do not contribute significantly to the observed behavior of the sum $P+V$ vs positron implantation energy. According to the above discussion the most important contribution to the term $N_{escaped}(E)$ in the present samples with nanochannels is expected to be the out-diffusion into the vacuum of *o*-Ps with high energy.

In Fig. 6 the curves $P(E)$ vs $V(E)$ measured in silicon and in some samples of the series realized by etching and subsequently reoxidation are shown. In silicon all the data, with the exception of those measured at very low positron implantation energy, are grouped around the point with coordinates $(V_{\mathrm{Si}}; P_{\mathrm{Si}})$. At the contrary, in the samples with nanochannels the behavior of the curves is different. For high positron implantation energy all the data lie along a straight line. This can be explained considering that *o*-Ps formed deep in the nanochannels (i.e., at high positron implantation energy E) has very low probability to out diffuse into the vacuum with

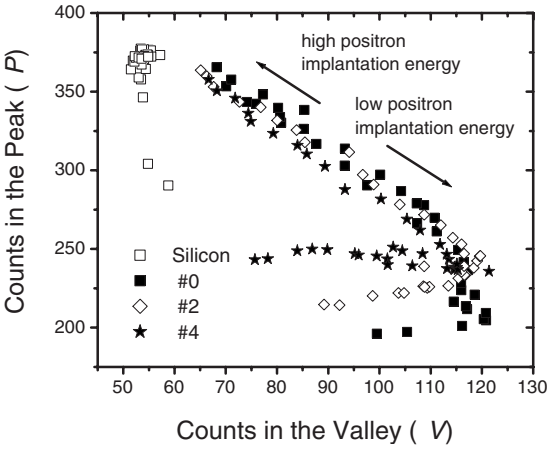

FIG. 6. $P(E)$ vs $V(E)$ curves in the unit of time measured in silicon and in samples #0, #2, and #4.

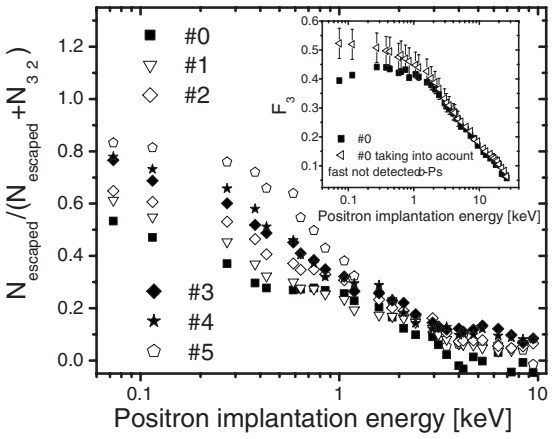

FIG. 7. Fraction $N_{escaped}(E)/[N_{2\gamma 3\gamma}(E)+N_{escaped}(E)]$ of counts due to fast o-Ps annihilations not detected by HpGe detector vs positron implantation energy. Errors $\pm 9\%$. Inset: $F_{3\gamma}(E)$ measured in sample #0 (squares, errors inside the point size) and corrected (triangles, error reported) by taking into account the presence of fast o-Ps not detected by the HpGe detector.

high velocity and to exit from the detection region because it reduces progressively its energy by collision with the walls of the nanochannels. Thus for high E values, $N_{escaped}(E)$ is negligible and using Eq. (1) the linear relationship $P(E) = P_{Si} - \alpha V(E) + \alpha V_{Si}$ is found. Fitting the linear part of the $P(E)$ vs $V(E)$ curves the term α and the coordinates $(V_{Si}; P_{Si})$ can be evaluated. They result $\alpha \sim 2.1 \pm 0.1$ and $(V_{Si}; P_{Si}) \sim (55 \pm 2; 370 \pm 2)$.

At low positron implantation energies the $P(E)$ vs $V(E)$ curves deviate from the linearity due to the presence of fast o-Ps out diffusing through the nanochannels. As expected this deviation is more appreciable in larger channels where an o-Ps atoms formed at a given depth can reach the vacuum with a smaller number of collisions with the surface of the nanochannels. Actually in the sample #4 (channel size 14–20 nm) the effect is more intense than in samples #0 (4–7 nm). Knowing the term α and the coordinates $(V_{Si}; P_{Si})$ it is possible to evaluate $N_{escaped}(E)$ by solving the system given by Eq. (1). One obtains $N_{escaped}(E) = P_{Si} - P(E) - \alpha[V(E) - V_{Si}]$, where $\alpha[V(E) - V_{Si}] = N_{2\gamma 3\gamma}(E)$.

The fraction $N_{escaped}(E)/[N_{2\gamma 3\gamma}(E)+N_{escaped}(E)]$, that is related to the fraction of fast o-Ps not detected by the HpGe detector, is reported in Fig. 7 for all the measured samples. The figure shows that the fast not-detected o-Ps increases with the size of the nanochannels and points out a strong correlation between the nanochannel size and the velocity of the emitted o-Ps.

In the sample #0 with the smallest pore diameter, the fraction $N_{escaped}(E)/[N_{2\gamma 3\gamma}(E)+N_{escaped}(E)]$ is about the 50% at low positron implantation energy and approaches to 0% around 5 keV. Increasing the diameter of the channel from 4–7 nm of sample #0 to 8–12 nm of sample #1, the term grows to 60% at low positron implantation energy and it becomes 65%, 75%, and 78 % in samples #2 (8–14 nm of pore size), #3 (10–16 nm), and #4 (14–20 nm), respectively. The fraction is up to 83% in sample #5 that has the largest channels (80–120 nm). Increasing the positron implantation energy above 6–7 keV the fraction decreases below 10% in all samples.

The presence of fast not-detected o-Ps at low positron implantation energy is also important when the fraction of implanted positron annihilating as o-Ps, $F_{3\gamma}(E)$, has to be correctly estimated. If one does not take into account the fast o-Ps, the $F_{3\gamma}(E)$ is appreciably underestimated at low positron implantation energy. As an example, in the inset of Fig. 7 the $F_{3\gamma}(E)$ curve measured in sample #0 is compared to the curve for the same sample but corrected taking into account the presence of fast not-detected o-Ps. The $F_{3\gamma}(E)$ (see experimental paragraph for definition) is recalculated for each E by adding $N_{escaped}(E)$ counts, weighted by the term α, to the valley area in the $R(E)$ parameter. In the corrected $F_{3\gamma}(E)$ curve, at very low E the true o-Ps fraction is around 53% of implanted positrons and it decreases monotonically by increasing the positron implantation energy. With the decrease in $N_{escaped}(E)$ the deviation with respect to the measured $F_{3\gamma}(E)$ curve diminishes and it disappears completely at around 5 keV. This result points out the importance of considering not-detected o-Ps to evaluate the o-Ps fraction at low E when studying porous samples with high emission of fast Ps into the vacuum. The experimental data of Fig. 3, corrected by the not-detected o-Ps, are reported in Fig. 8.

D. o-Ps diffusion length vs nanochannel dimensions

In order to found the fraction of o-Ps out diffusing at each positron implantation energy and the o-Ps diffusion length, the corrected $F_{3\gamma}(E)$ curves have been fitted with a diffusion model. We modified a model first proposed to study the o-Ps formation and out-diffusion in ice[32] and then adapted to the o-Ps diffusion in porous materials.[43]

It is important to emphasize that the adopted model is based on the diffusion equation which assumes a constant velocity of o-Ps into the pores. Currently no models of o-Ps based on Boltzmann equation that takes into account the energy loss of Ps hitting the nanochannels surfaces have been developed. In spite of this limitation diffusion models were found to give reliable fit with constant o-Ps diffusion in ordered and disordered porous materials.[18,25] Indications about

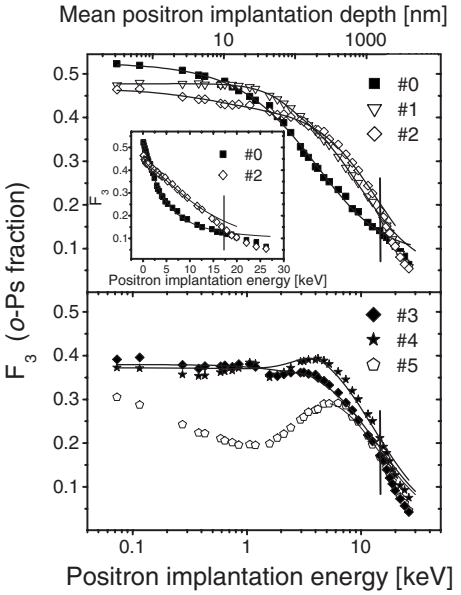

FIG. 8. $F_{3\gamma}(E)$ data of Fig. 3 corrected for the not-detected fast o-Ps atoms emitted by the nanochannels. The error on $F_{3\gamma}$ is $\pm 10\%$ up to 5 keV then it is $\pm 3.5\%$. The continuous lines through the points are best fits obtained by the diffusion model described in the text. The vertical lines mark the border between the silicon region with nanochannels and the bulk silicon. The inset in the upper panel shows $F_{3\gamma}(E)$ curves for #0 and #2 with positron implantation energy in linear scale.

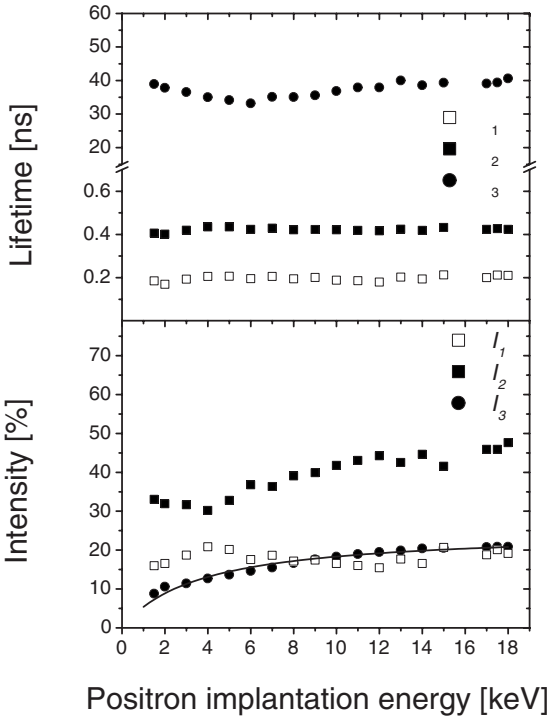

FIG. 9. Lifetime measurements performed on a sample similar to #0. Lifetimes (upper panel) and intensities (lower panel) as a function of positron implantation energy. Errors are inside the size of the points. The continuous line through the I_3 component (intensity of the pickoff annihilations) is a best fit with a logistic curve.

the fraction of o-Ps annihilating via 3γ in the pores, the amount of o-Ps emitted into the vacuum and the length of diffusion of o-Ps.

The corrected $F_{3\gamma}(E)$ curves, shown in Fig. 8, were fitted by the following equation:

$$F_{3\gamma}(E) = A(E) \cdot B(E) + C(E), \tag{2}$$

$A(E)$ is a phenomenological profile for o-Ps formation,

$$A(E) = F_1 + (F_2 - F_1)e^{-1/2(E/E_1)^{\beta}}, \tag{3}$$

where F_1, F_2, β, and E_1 are fitting parameters. At low positron implantation energy, $A(E)$ takes into accounts for all channels of o-Ps formation at the surface,

$$B(E) = \frac{1}{1 + \left(\frac{E}{E_0}\right)^{1.6}} \tag{4}$$

is the probability of o-Ps out-diffusion from the nanochannels where $E_0 = \sqrt[1.6]{L_{Ps}\rho/40}$.[3,32]

The product $A(E) \cdot B(E)$ gives the fraction of formed o-Ps that annihilate into 3γ after being emitted into vacuum. The last term, $C(E)$, is the fraction of the formed o-Ps that annihilate by 3γ into pores. This fraction is expected to increase from a low value near the surface and to reach a constant value in depth. The lower value near the surface is because of the increasing fraction of o-Ps out diffusing into the vacuum. This behavior is similar to that of o-Ps annihilating by pickoff. A lifetime measurement was performed in a not-capped sample similar to #0 and the functional form for the $C(E)$ term was assumed as proportional to the intensity of the pickoff component. The measured lifetimes and their intensities are shown in Fig. 9. Because the lifetime system does not detect three gamma annihilations, at each positron implantation energy the lifetime intensities were renormalized taking into account the $F_{3\gamma}(E)$.

The lifetime τ_3 corresponding to pickoff annihilations is around 37 ns and its intensity I_3 increases smoothly from the surface to the bulk. The $\tau_1 \sim 190$ ps and its intensity I_1 are due to p-Ps annihilations and positrons annihilation in silicon. The $\tau_2 \sim 420$ ps and its intensity I_2 come from positrons annihilating into silica and at the silica surfaces.

The functional form describing the I_3 component, and assumed for $C(E)$, is a logistic curve,

$$C(E) = K\left[\frac{C_1 - C_2}{1 + \left(\frac{E}{E_2}\right)} + C_2\right], \tag{5}$$

where the constants C_1, C_2, and E_2 were evaluated by fitting $I_3(E)$ (see Fig. 9) and K is the proportional factor.

All samples, except #5, can be well fitted with the above model. The best fits are shown as continuous lines in Fig. 8. #5 can be only modeled from 5 keV positron implantation energy, probably due to a strong modification of the surface with respect to the other sample (seen SEM pictures in Fig. 4). In sample #0 the model points out that the fraction of o-Ps annihilating in the nanochannels via 3γ is about 5% of implanted positrons at 4 keV and increases slightly up to less

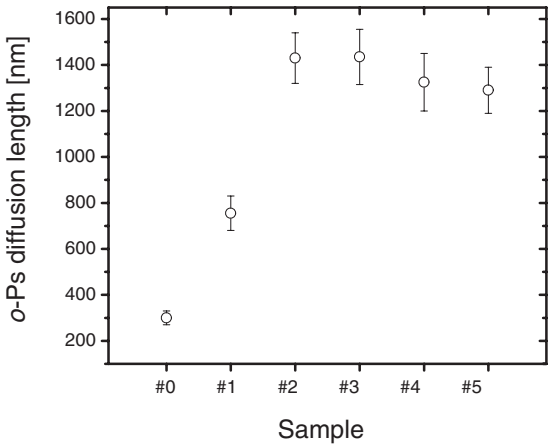

FIG. 10. *o*-Ps diffusion length in samples #0, #1, #2, #3, #4, and #5 obtained by fitting the corrected $F_{3\gamma}(E)$ curves with the diffusion model described in the text. Errors ±10%.

than 7% at higher energies. The *o*-Ps reaching the vacuum through the nanochannels is up to 42% of implanted e^+ at ~1 keV. The *o*-Ps fraction out diffusing at 10 keV positron implantation energy is still 10%.

Increasing the nanochannels diameter, the fraction of implanted positrons annihilating as *o*-Ps via 3γ into nanochannels at high depth decreases (<4% in #1) and almost disappears after 2 cycles (<1% in #2, #3, #4, and #5). According to these results the fraction of *o*-Ps emitted into the vacuum at ~1 keV is up to 40% in #1 and it does not decrease considerably not even in samples #2, #3, and #4 (35–36 %). These values are comparable to the best results reported up to now in literature and obtained in disordered mesoporous cetyl trimethyl ammonium chloride (CTACl)-tetraethoxylane (TEOS) films synthesized by spin coating with TEOS as source for the silica network and CTACl as porogen.[17] Moreover, due to the decreasing of the fraction of *o*-Ps annihilating via 3γ in the channels, the *o*-Ps fraction out diffusing at 10 keV positron implantation energy (corresponding to 800 nm depth) is still 17% in #1 and up to 23–25 % in #2, #3, #4, and #5. As a comparison in mesoporous silica materials the *o*-Ps out diffusing decreases quickly just above 4 keV positron implantation energy.[14,16,17] Inside the errors, Eq. (2) points out a constant Ps formation in all samples from the bulk to the surface.

The *o*-Ps diffusion length $L_{Ps}=\frac{40}{\rho}E_0^{1.6}$, extracted by the fitting procedure, is shown in Fig. 10 as a function of the etching+oxidation cycles. A variation in the channel dimension from few to tens of nanometer induces a strong modification of the *o*-Ps diffusion length. The *o*-Ps diffusion length starts from a value of 300 ± 30 nm in sample #0 then it increases to 780 ± 80 nm in sample #1 and to 1430 ± 140 nm in sample #2. After further cycles (#3, #4, and #5), the *o*-Ps diffusion length attains an almost constant value.

It is worth to note, as found also in Ref. 18, that the data are well described in all samples by a constant diffusion length L_{Ps} in spite of the fact that Ps changes its velocity during its diffusion path. It is also important to outline that without correcting the measured $F_{3\gamma}(E)$ for the fast *o*-Ps, the same L_{Ps} values can be obtained by fitting the $F_{3\gamma}(E)$ points above 2 keV in samples #0, #1, and #2 and above 5–6 keV in samples #3, #4, and #5, where the fraction of *o*-Ps annihilating via 3γ and the *o*-Ps formation achieve an almost constant values.

E. *o*-Ps cooling and nanochannel dimension

The possibility to control the dimension of the nanochannels from few nanometers up to 20–50 nm preserving a very high emission of *o*-Ps into the vacuum is of great importance in the cooling of *o*-Ps to low temperature. In fact, as discussed in Ref. 26 (see also Ref. 18), the ground state of *o*-Ps and consequently the minimum temperature that it can reach in a pore by loosing its energy colliding with walls depends on the dimension of the pore itself. If we approximate each nanochannel as an infinitive potential well of cuboidal shape with a quadratic base of side a and infinite length along the direction perpendicular to the surface of the sample, the minimum energy of *o*-Ps is given by $E=\frac{\hbar^2\pi^2}{ma^2}$ and the minimum temperature is $T=\frac{2}{3k_B}\frac{\hbar^2\pi^2}{ma^2}$ (m is the mass of *o*-Ps, k_B is the Boltzmann constant, and $\hbar$ is the reduced Planck constant). This means that in nanochannels with side of 5 nm, *o*-Ps cannot be cooled at temperature lower than 116 K. Increasing the size of the nanochannels the minimum accessible temperature decreases and, in nanostructures of 20 nm, it is around 7 K. On the other hand, the increase in the size of nanochannels is expected to extend the thermalization time of *o*-Ps,[26,39] thus it is necessary to optimize the nanochannel dimension to reach the *o*-Ps temperature required by the final application.

The value of the constant diffusion coefficient $D_{Ps}=L_{Ps}^2/\tau$ can be estimated in samples with different nanochannel dimension by using the Ps lifetimes (τ) calculated in channels by the rectangular extension of the Tao-Eldrup model[44] and the diffusion length L_{Ps} reported in Fig. 10. The D_{Ps} values 0.012 ± 0.002 cm^2/s, 0.060 ± 0.008 cm^2/s, 0.18 ± 0.02 cm^2/s, 0.18 ± 0.02 cm^2/s, 0.13 ± 0.02 cm^2/s, and 0.13 ± 0.02 cm^2/s are found for the samples #0, #1, #2, #3, #4, and #5, respectively. These diffusion constants, except that of sample #0, are from two to four times higher than the diffusion constant found in disordered porous silica samples (see, for example, Ref. 18). In TOF measurements at RT performed on a sample with nanochannels dimensions between that of #0 and #1,[25] 19% of out diffusing *o*-Ps was found to escape thermalized into the vacuum when implanting positrons at 7 keV energy. A mean time of permanence in the channels of about 16 ns was evaluated by the equation $\bar{t}=\bar{z}^2/(2D_{Ps})$ (Ref. 18) for thermalized *o*-Ps. This time is about two times the thermalization time at RT.[39] Because of increasing the nanochannel dimensions an increase in the thermalization time is expected[39] we can estimate that for obtaining thermalized *o*-Ps in samples #3, #4, and #5, positrons would be implanted at an energy above 9.5 keV (~770 nm depth). At these energies there is still about 20% out diffusing *o*-Ps and about 3% of thermalized *o*-Ps could be predicted at RT. A sensible fraction of thermalized *o*-Ps is also expected at cryogenic temperature although from

slightly higher depth due to the increase in the thermalization time.[26]

In addition to the possibility to modify the nanochannels dimension, samples obtained with the described procedure could offer further advantages in the production of *o*-Ps at low temperature with respect to the porous silica samples investigated until now. Present samples are prevalently constituted by silicon with a thin layer of silica on the channels surface, therefore the resistivity of these samples is lower than that of sample composed only of silica. For this reason they are expected to be less sensitive to charging effects due to intense positron pulse implantation. Moreover, in silica at low temperature, paramagnetic centers are known to be formed under intense positron irradiation and to induce *o*-Ps quenching by *o*-Ps$\rightarrow$*p*-Ps conversion.[45] Because of the high ratio between silicon and silica, the formation of paramagnetic centers is expected to be less important. The major effect would be due to paramagnetic centers formed on the surface[46] of the nanochannels that could increase the *o*-Ps lost during the cooling process.

IV. CONCLUSION

It was shown that silicon samples with ordered array of oxidized nanochannels when implanted with positrons give rise to high yield and abundant emission into the vacuum of *o*-Ps. This material can be used as efficient positron-*o*-Ps converter. Analyzing the decrease in the counts in the 511 keV peak and valley areas of the detected gamma ray spectrum, the fraction of fast *o*-Ps leaving the samples has been estimated. A well distinguishable variation in the amount of fast *o*-Ps emitted from regular nanochannels has been appreciated by varying their size by few nanometers. The estimate of the not-detected emitted fast *o*-Ps was also shown to be important in the correct evaluation of the fraction of implanted positrons forming *o*-Ps, $F_{3\gamma}(E)$, in samples with high Ps emission. With respect to target realized with silica, in which the connected porosities toward the vacuum are disordered, this converter could offer many advantages. The possibility to modify the dimension of the nanochannels preserving *o*-Ps emission into the vacuum would allow *o*-Ps cooling at cryogenic temperature. At present only oxidation in air of the produced nanochannels was investigated. In future different type of oxidation could be explored to correlate the quality of the grown oxide with the Ps yield, furthermore the silicon termination at the walls of the nanochannels could be controlled by different type of gas exposure for improving Ps energy loss.

ACKNOWLEDGMENTS

We acknowledge A. Miotello and L. Pavesi for the kindly availability of their laboratories for SEM measurements and for the nanoporous material production, respectively; W. Egger and L. Ravelli for lifetime measurements. One of the authors, P.B., acknowledges PAT support through GOPSI project.

*mariazzi@science.unitn.it

[1] S. Berko and H. N. Pendleton, Annu. Rev. Nucl. Part. Sci. **30**, 543 (1980).

[2] A. P. Mills, Jr., in *Positron Solid-State Physics*, edited by W. Brandt and A. Dupasquier (North-Holland, Amsterdam, 1983), p. 432; K. G. Lynn, *Positron Solid-State Physics*, edited by W. Brandt and A. Dupasquier (North-Holland, Amsterdam, 1983), p. 609.

[3] P. J. Schultz and K. G. Lynn, Rev. Mod. Phys. **60**, 701 (1988).

[4] D. W. Gidley, K. G. Lynn, M. P. Petkov, M. H. Weber, J. N. Sun, and A. F. Yee, in *New Directions in Antimatter Chemistry and Physics*, edited by C. M. Surko and F. A. Gianturco (Kluwer Academic, Dordrecht, 2001), p. 151.

[5] H. K. M. Tanaka, Y. Yamauchi, T. Kurihara, Y. Sakka, K. Kuroda, and A. P. Mills, Jr., Adv. Mater. **20**, 4728 (2008).

[6] D. B. Cassidy and A. P. Mills, Jr., Nature (London) **449**, 195 (2007).

[7] A. P. Mills, Jr., Radiat. Phys. Chem. **76**, 7 (2007).

[8] H. Iijima, T. Asonuma, T. Hirose, M. Irako, T. Kumita, M. Kajita, K. Matsuzawa, and K. Wada, Nucl. Instrum. Methods Phys. Res. A **455**, 104 (2000).

[9] P. M. Platzman and A. P. Mills, Jr., Phys. Rev. B **49**, 454 (1994).

[10] D. B. Cassidy and A. P. Mills, Jr., Phys. Status Solidi C **4**, 3419 (2007).

[11] P. Perez and A. Rosowsky, Nucl. Instrum. Methods Phys. Res. A **545**, 20 (2005).

[12] A. Kellerbauer, M. Amoretti, A. S. Belov, G. Bonomi, I. Boscolo, R. S. Brusa, M. Büchner, V. M. Byakov, L. Cabaret, C. Canali, C. Carraro, F. Castelli, S. Cialdi, M. de Combarieu, D. Comparat, G. Consolati, N. Djourelov, M. Doser, G. Drobychev, A. Dupasquier, G. Ferrari, P. Forget, L. Formaro, A. Gervasini, M. G. Giammarchi, S. N. Gninenko, G. Gribakin, S. D. Hogan, M. Jacquey, V. Lagomarsino, G. Manuzio, S. Mariazzi, V. A. Matveev, J. O. Meier, F. Merkt, P. Nedelec, M. K. Oberthaler, P. Pari, M. Prevedelli, F. Quasso, A. Rotondi, D. Sillou, S. V. Stepanov, H. H. Stroke, G. Testera, G. M. Tino, G. Trénec, A. Vairo, J. Vigué, H. Walters, U. Warring, S. Zavatarelli, D. S. Zvezhinskij, and AEGIS Proto-Collaboration, Nucl. Instrum. Methods Phys. Res. B **266**, 351 (2008).

[13] R. S. Yu, T. Ohdaira, R. Suzuki, K. Ito, K. Hirata, K. Sato, and Y. Kobayashi, Appl. Phys. Lett. **83**, 4966 (2003).

[14] K. Ito, R. S. Yu, K. Sato, K. Hirata, and Y. Kobayashi, J. Appl. Phys. **98**, 094307 (2005).

[15] H. K. M. Tanaka, T. Kurihara, and A. P. Mills, Jr., J. Phys.: Condens. Matter **18**, 8581 (2006).

[16] C. He, T. Ohdaira, N. Oshima, M. Muramatsu, A. Kinomura, R. Suzuki, T. Oka, and Y. Kobayashi, Phys. Rev. B **75**, 195404 (2007).

[17] L. Liszkay, M. F. Barthe, C. Corbel, P. Crivelli, P. Desgardin, M. Etienne, T. Ohdaira, P. Perez, R. Suzuki, V. Valtchev, and A. Walcarius, Appl. Surf. Sci. **255**, 187 (2008).

[18] D. B. Cassidy, P. Crivelli, T. H. Hisakado, L. Liszkay, V. E.

Meligne, P. Perez, H. W. K. Tom, and A. P. Mills, Jr., Phys. Rev. A **81**, 012715 (2010).
[19] S. Van Petegem, C. Dauwe, T. Van Hoecke, J. De Baerdemaeker, and D. Segers, Phys. Rev. B **70**, 115410 (2004).
[20] R. S. Vallery, P. W. Zitzewitz, and D. W. Gidley, Phys. Rev. Lett. **90**, 203402 (2003).
[21] L. Liszkay, C. Corbel, P. Perez, P. Desgardin, M. F. Barthe, T. Ohdaira, R. Suzuki, P. Crivelli, U. Gendotti, A. Rubbia, M. Etienne, and A. Walcarius, Appl. Phys. Lett. **92**, 063114 (2008).
[22] T. Maruo, S. Tanaka, H. W. Hillhouse, N. Nishiyama, Y. Egashira, and K. Ueyama, Thin Solid Films **516**, 4771 (2008).
[23] *Positron Solid-State Physics*, edited by W. Brandt and A. Dupasquier (North-Holland, Amsterdam, 1983).
[24] R. Krause-Rehberg and H. S. Leipner, *Positron Annihilation in Semiconductors* (Springer, New York, 1998).
[25] S. Mariazzi, P. Bettotti, and R. S. Brusa, Phys. Rev. Lett. (to be published 2010).
[26] S. Mariazzi, A. Salemi, and R. S. Brusa, Phys. Rev. B **78**, 085428 (2008).
[27] O. Bisi, S. Ossicini, and L. Pavesi, Surf. Sci. Rep. **38**, 1 (2000).
[28] A. Zecca, M. Bettonte, J. Paridaens, G. P. Karwasz, and R. S. Brusa, Meas. Sci. Technol. **9**, 409 (1998).
[29] C. Macchi, S. Mariazzi, G. P. Karwasz, R. S. Brusa, P. Folegati, S. Frabboni, and G. Ottaviani, Phys. Rev. B **74**, 174120 (2006).
[30] R. S. Brusa, C. Macchi, S. Mariazzi, and G. P. Karwasz, Acta Phys. Pol. A **107**, 702 (2005).
[31] A. P. Mills, Jr., Phys. Rev. Lett. **41**, 1828 (1978).
[32] M. Eldrup, A. Vehanen, P. J. Schultz, and K. G. Lynn, Phys. Rev. B **32**, 7048 (1985).
[33] E. Soininen, A. Schwab, and K. G. Lynn, Phys. Rev. B **43**, 10051 (1991).
[34] P. Sperr, W. Egger, G. Kögel, G. Dollinger, C. Hugenschmidt, R. Repper, and C. Piochacz, Appl. Surf. Sci. **255**, 35 (2008).
[35] C. Hugenschmidt, G. Dollinger, W. Egger, G. Kögel, B. Löwe, J. Mayer, P. Pikart, C. Piochacz, R. Repper, K. Schreckenbach, P. Sperr, and M. Stadlbauer, Appl. Surf. Sci. **255**, 29 (2008).
[36] Y. Nagashima, Y. Morinaka, T. Kurihara, Y. Nagai, T. Hyodo, T. Shidara, and K. Nakahara, Phys. Rev. B **58**, 12676 (1998).
[37] R. S. Brusa, C. Macchi, S. Mariazzi, G. P. Karwasz, W. Egger, P. Sperr, and G. Kögel, Phys. Rev. B **71**, 245320 (2005).
[38] G. Brauer, W. Anwand, W. Skorupa, A. G. Revesz, and J. Kuriplach, Phys. Rev. B **66**, 195331 (2002).
[39] Y. Nagashima, M. Kakimoto, T. Hyodo, K. Fujiwara, A. Ichimura, T. Chang, J. Deng, T. Akahane, T. Chiba, K. Suzuki, B. T. A. McKee, and A. T. Stewart, Phys. Rev. A **52**, 258 (1995).
[40] A. P. Knights and P. G. Coleman, Surf. Sci. **367**, 238 (1996).
[41] J. A. Baker and P. G. Coleman, J. Phys. C **21**, L875 (1988).
[42] R. H. Howell, I. J. Rosenberg, and M. J. Fluss, Phys. Rev. B **34**, 3069 (1986).
[43] M. P. Petkov, M. H. Weber, K. G. Lynn, and K. P. Rodbell, Appl. Phys. Lett. **79**, 3884 (2001).
[44] T. L. Dull, W. E. Frieze, D. W. Gidley, J. N. Sun, and A. F. Yee, J. Phys. Chem. B **105**, 4657 (2001).
[45] H. Saito, Y. Nagashima, T. Hyodo, and T. Chang, Phys. Rev. B **52**, R689 (1995).
[46] D. B. Cassidy, K. T. Yokoyama, S. H. M. Deng, D. L. Griscom, H. Miyadera, H. W. K. Tom, C. M. Varma, and A. P. Mills, Jr., Phys. Rev. B **75**, 085415 (2007).